



Combination of remote-sensing spectral indices to classify the areas of land degradation in West Burdwan district, India

Sabyaschi Kabiraj¹ · Elanchezhyan Duraisekaran¹ · Malarvizhi Ramaswamy¹

Received: 30 August 2021 / Accepted: 9 March 2022 / Published online: 31 March 2022
© The Author(s), under exclusive licence to Springer-Verlag GmbH Germany, part of Springer Nature 2022

Abstract

Demarcating the extent of land degradation remains a major challenge worldwide. A combination of remote-sensing spectral indices and Land Degradation Index (LDI) were used for the delineation and classification of land degraded areas in West Burdwan district, West Bengal, India. Mining, brick and other industries were delineated using the maximum likelihood classification (MLC) algorithm of the supervised image classification method. Land Surface Temperature (LST), Normalized Difference Vegetation Index (NDVI), Soil Moisture Index (SMI), night-time LST and Evapotranspiration (ET) were used as indicators of land degradation and were derived from Landsat and Moderate Resolution Imaging Spectroradiometer satellite images for the years from 1990 to 2020. The result indicates an increase in industrial area from 2.06% to 7.62% of the district area from 1990 to 2020. Our pixel-based time-series analysis displays some considerable land degradation over the past 30 years, including (i) increasing daytime LST, (ii) declining vegetation, (iii) decreasing ET. However, no considerable change was found in night-time-LST and SMI. A strong positive correlation (adjusted $R^2 > 0.5$ and $p < 0.05$) was observed between mining area expansion and daytime LST and a negative correlation between mining area expansion and NDVI and ET respectively. LDI shows a total land degradation of 91.01 km² over the entire study region. Mining area expansion was found to be one of the major stressors to local environmental degradation. The results from this study may help the decision-makers and policymakers to provide a better management plan for sustainable land management in future.

Keywords Normalized Difference Vegetation Index · Soil Moisture Index · Land Degradation Index · Geographical information system

Introduction

The decline of the land productivity due to the direct or indirect processes resulting in the diminishing of the ecological services of the environment is termed as Land degradation (UNCCD 1994; Adamo and Crews-Meyer 2006). The causes of land degradation can be either biophysical or human-induced or both (Sklenicka 2016). Increasing population, loss of forest and vegetation cover and soil erosion

are the major causes of land degradation (Taddese 2001; Gao and Liu 2010; Abu Hammad and Tumeizi 2012). Globally, ~24% of the land is affected by severe land degradation (Pacheco et al. 2018). Most studies on land degradation in Asia have focused on the Middle East (Faour 2014). Some has also examined the temperate regions of China and Mongolia (Gong et al. 2014).

In a developing country, such as India, 96 million hectares of land (about 30%) are affected by land degradation (ISRO 2018). In West Bengal, a state of India, about 19.54% of the total geographical area is affected by land degradation (ISRO 2016). The West Burdwan district of West Bengal state is affected by land degradation processes mainly through the conversion of agricultural land to urbanization and industrialization such as coalfield, brick industries etc. (Ghorai et al. 2018). Understanding the previous environmental drivers of land use expansion, addressing current conditions using geospatial tools and providing scientific future forecasts

This article is part of a Topical Collection in Environmental Earth Sciences on Earth Surface Processes and Environment in a Changing World: Sustainability, Climate Change and Society, guest edited by Alberto Gomes, Horácio García, Alejandro Gomez, Helder I. Chaminé.

✉ Sabyaschi Kabiraj
sabyaschi.kabiraj2@gmail.com

¹ Department of Civil Engineering, Anna University, Chennai, Tamil Nadu, India

helps resource managers in planning and maintaining natural resources (Mohd Ayob et al. 2015).

Remote Sensing (RS) and Geographic Information System (GIS) aid in identifying areas of land degradation with significant spatial information (Cheung et al. 2021; Thiam 2003). The ability of remote-sensing technology to see targets better than the human eye makes it a powerful tool for studying the dynamics on the earth's surface (Higginbottom and Symeonakis 2014). Satellite imagery can cover large and inaccessible areas and can provide a repeatable collection of long-term land degradation indicators (Mohapatra et al. 2014). RS spectral indices show changes in land surface, vegetation productivity, the effect of long-term climate variability and variation in physico-chemical properties of soil. Long-term profiles of the relationship between vegetation dynamics and Land Use / Land Cover (LULC) change can provide valuable information for understanding land degradation processes (Shalaby and Tateishi 2007; Matin et al. 2018). This relationship is complex, where vegetation recovers faster than soil. A permanent land change can only occur if the vegetation itself is severely degraded or the soil becomes infertile. The continued change could further influence regional climates and intensify ongoing land degradation (Lambin et al. 2003).

Researchers have used many remote-sensing-derived indicators using different satellite images to characterize land degradation. Vlek et al. (2008, 2010) examined the long-term trends of the Normalized Difference Vegetation Index (NDVI) concerning the annual dynamics of rainfall and atmospheric fertilization to determine the extent to which humans affect net primary productivity. Lanorte et al. (2014) used the NDVI time series to monitor vegetation recovery following fire disturbance at two test sites in Spain and Greece. Remote sensing is also used in vulnerability analysis (Oldeman et al. 1991; Lynden and Oldeman 1997; Sepehr et al. 2007; Bai et al. 2008; Masoudi and Zakeri Nejad 2010; Hein et al. 2011; D'Odorico et al. 2013; Masoudi 2014; Masoudi and Amiri 2015), which focuses on spatial models to assess desertification and land degradation. Lasanta et al. (2000) analyzed forest fragmentation using remote-sensing information and consider geospatial science as a useful tool for accessing changes in land quality. Milanović et al. (2017) presented the impact of anthropogenic factors such as mining activity, industrialization, construction and agricultural activities which leads to exploitation of land resources and suggested a more sustainable ecosystem using Landsat 5 imageries. Manjunatha and Basavarajappa (2020) noticed the degradation of land from the Survey of India (SoI) toposheet as well as LISS-III multispectral and geo-coded False Color Composite (FCC) of IRS-1D mapping and found that change in vegetation have an impact on surface runoff. Rahaman et al. (2020) framed that the land transformation due to natural as well as anthropogenic driving forces

especially industrialization by investigating Land Surface Temperature (LST), NDVI, Normalized Difference Water Index (NDWI), Leaf Area Index (LAI), Effective Roughness Length (ERL), and Surface Albedo (SA) indices. The above mentioned indices were correlated to see the difference in the eco-system response using Landsat and Moderate Resolution Imaging Spectroradiometer (MODIS) products. The observed effects are increasing temperature, decreasing evapotranspiration (ET), loss of productivity potential and biodiversity. Reversing land degradation is essential in solving the United Nations Sustainable Development Goal 15 (such as restoring degraded lands, combating desertification) (Lorenz et al. 2019). Although the global development issue of land degradation has been accepted no proper consensus has been arrived concerning its monitoring (Jong et al. 2011) mainly due to the site-specific nature of the problem. The present study will help in mapping and monitoring of degraded lands which finally will help in making plans to improve or develop remedial measures for degraded lands.

Worldwide various studies have been carried out to assess land degraded areas by quantifying - variation in LST, LULC change, urbanization and industrialization using remote sensing and GIS technology. Teodoro et al. (2021) used unmanned aerial vehicles (UAV) for land use, vegetation and altimetric mapping to monitor the environment. Das (2020) used Landsat 5-TM, Landsat 7-ETM+ and Landsat 8-OLI TIRS to assess the geo-environmental changes such as loss of soil fertility, riverbank erosion, river course changes, land degradation, water pollution, and health hazard of the workers due to brick kiln industrialization on the sides of the river. The unscientifically planned impacts and effects were analyzed by statistical techniques, sinuosity index, and water quality index. Joshi et al. (2009) conducted an Environmental Impact Assessment (EIA) and concluded that rapid industrialization and deforestation resulted in a highly vulnerable landscape considering the Landsat Multi-Spectral Scanner (MSS) as baseline data. Due to the lowering in vegetation area enormously owing to the unplanned expansion of the mining area, the adverse impacts on environmental pollution had reached a critical stage (Chitade and Katyar 2010). Das et al. (2020) projected that the increase in temperature due to major factors of urbanization and industrialization is in response to economic development. The economic development had resulted in LULC change as well as an increase in LST. Hamid et al. (2020) computed the eco-system using various Landsat products to study the vulnerability using LULC, Digital Elevation Model (DEM), soil, slope and geology combined with climate change due to industrialization in arid and semi-arid regions. The results showed that the grasslands are being subjected to high vulnerability rather than vegetation. Information can be extracted in different spatial and temporal scales and in addition, the model can be modified and then recalibrated

with the latest data on the current state of the environment (De Jong 1994; Boer 1999).

All the previous literature elucidated that Landsat image-eries are very useful in the delineation of degraded land in addition to MODIS data products. Although, the research carried out has focused particularly on land transformations, vegetation degradation or deforestation, LST changes using Landsat and MODIS data, very few studies focused on land degradation using multiple indicators, such as NDVI, LST, ET, LULC and Soil Moisture Index (SMI). A combination of all these indicators will give a better understanding of the land as each indicator have different spectral characteristics and output. Demarcation of land degradation areas and their magnitude has also been studied by very few researchers.

Numerous studies have been carried out over the West Burdwan district, such as Choudhury et al. (2019) focused on land use and land cover change and its impact on LST over the Asansol–Durgapur development region. Maity et al. (2020) assessed the impact of LULC changes on LST in Asansol municipality areas. Siddique et al. (2020) estimated the green space change around Asansol city, West Bengal and showed the impact of NDVI change on LST. Dutta et al. (2020) studied urban growth through land-use change dynamics from the years 1990–2010 in Kanksa block of Paschim Burdwan District.

All the previous works of literature mainly focused on LULC transformation and its impact on the LST at the district level or block level. Some studies focused on vegetation changes using NDVI. However, from our knowledge, none of the literature can explain the industrial expansion and its impact on land degradation at the micro-level. Long term monitoring of industrial expansion and its impact on land degradation indicators, such as ET, LST and vegetation index at the micro-level is very much important, as it is required to evaluate the environmental health status of the surrounding region. In addition, it helps to identify degrading regions spatially, which finally helps to take necessary actions to reduce the impact and thus consider environmentally sustainable solutions in the future. In this study, it is attempted to quantify the industrial expansion spatially for the past 30 years and also, to build a model to identify and spatially classify degraded land areas of West Burdwan district of West Bengal, India. The objectives of the study are (a) to demarcate the areas of land degradation using various spectral indices and (b) to classify the varying magnitude of land degradation using the land degradation index.

Study area

Paschim Burdwan is a district in West Bengal, India formed by the bifurcation of the erstwhile Burdwan District. West Burdwan district (Paschim meaning “West” in Bengali) is an extension of Chota Nagpur plateau with an area of 1817 km². The district is bounded in the north by Ajay River and in the south by Damodar River both flowing eastwards into the Bay of Bengal. The population of the district increased from 25, 52,781 in the year 2001 to 28, 82,031 in 2011 with a decadal growth of 12.90% (Choudhury et al.2019). According to the Indian Meteorological Department, the climate of the district is sub-tropical monsoon type with hot summer, mild winter, dry winter which belongs to Cwa type climate of Koppen’s classification, with a maximum summer time temperature of 44 °C. The average annual rainfall of the district is 1408 mm. The district has two subdivisions, namely, Asansol Sadar and Durgapur, and is one of the premier Indian districts in value of minerals. The index map of the study area along with the mining, brick and other industries is shown in Fig. 1.

Asansol is the 39th largest urban agglomeration in India, whereas Durgapur is the most industrialized city in eastern India. Asansol is situated over the largest coal reserve in the country with the best type of non-coking coal reserve in the nation. Raniganj coalfield in the district was the birthplace of the Indian coal industry and contributed to the industrialization of the subdivision. Though the coal industries were exposed in the early eighteenth century, the region was not developed until the mid-nineteenth century. The industrial development led to the forest clearance in the western part of the district, while eastern part forests still exist in Kanksa and adjoining Faridpur, Ukhra areas.

This industrialization led to most of the forests in the western part being cleared, while in the eastern part, forests still exist in Kanksa (Ramnabagan wildlife sanctuary) and its adjoining Faridpur and Ukhra areas. Durgapur steel plant, Durgapur thermal power station and ISSCO steel plant along with hundreds of large, medium and small-scale industries have dotted the Durgapur subdivision of the district giving the district an industrial identity in eastern India. The unit industrial growth increased from 143 to 840 in the 6 years from 2006 to 2012 resulting in Durgapur emerging as an industrial urban centre of West Bengal. The geology map of the West Burdwan district is represented in Fig. 2.

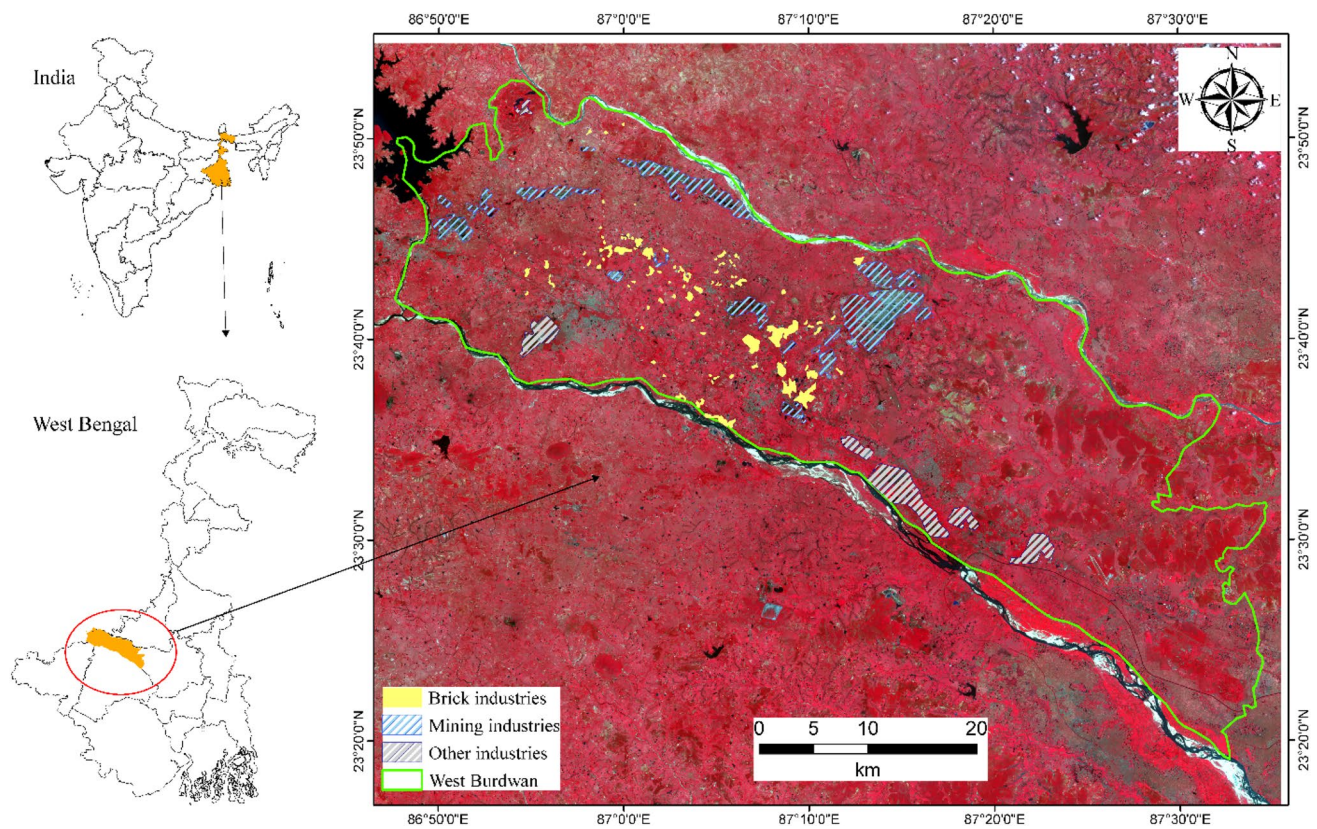


Fig. 1 Study area map

Materials and methods

Satellite data

This study used Landsat 5 Thematic Mapper (TM) and Landsat 8 Operational Land Imager (OLI) and Thermal Infrared Sensor (TIRS) imageries (spatial resolution 30 m) at 5 years of equal intervals from 1990 to 2020. We choose 30 years, because the West Burdwan district has experienced rapid industrial growth in between that time period. A 30-year period is useful for examining long-term trends, but it may average out multiple short-term changes (e.g., disturbed or cleared vegetation becomes re-established), so, we studied short-term changes of 5-year intervals as well over the study area.

Two best quality imageries (cloud cover less than 10%) one in summer season (March–May) and another in the winter season (December–February) of the years 1990, 1995, 2000, 2005, 2010, 2015 and 2020 (Table 1) downloaded from the USGS website (<https://earthexplorer.usgs.gov/>) were selected for the study to minimize the seasonal and spectral variation. As Landsat satellite mission provides free data with the largest time coverage from 1972 up to the

present and most of the researchers used Landsat data for land degradation studies, we also used Landsat data for our studies as well because of its coverage from the years 1990 to 2020. Each band of the satellite image were radiometrically corrected using ERDAS Imagine 2015 and thus used to calculate NDVI, SMI and seasonal daytime LST for the study area.

We also used MODIS level-2 data product at 1 km spatial resolution for land degradation indicators, which cannot be directly derived from Landsat imagery. Specifically, we used MODIS 8-day product from 2000 to 2020 to compute seasonal night-time LST. The study area comes under 2 scenes of MODIS satellite imagery. Seasonal night-time LST was derived by compositing MODIS 8-day-LST product (MOD11A2) from 2000 to 2020 (at 5-year equal interval) to arrive mean values of summer and winter night-time LST for the years 2000, 2005, 2010, 2015 and 2020, respectively. The methodology detail of the present study is given in the flow chart (Fig. 3).

MODIS yearly ET product (MODIS16A3) from 2000 to 2014 were used to evaluate dynamics of water deficit due to evaporation from soil and transpiration from the plants (Mu et al. 2007). As the MODIS 16A3 annual ET satellite

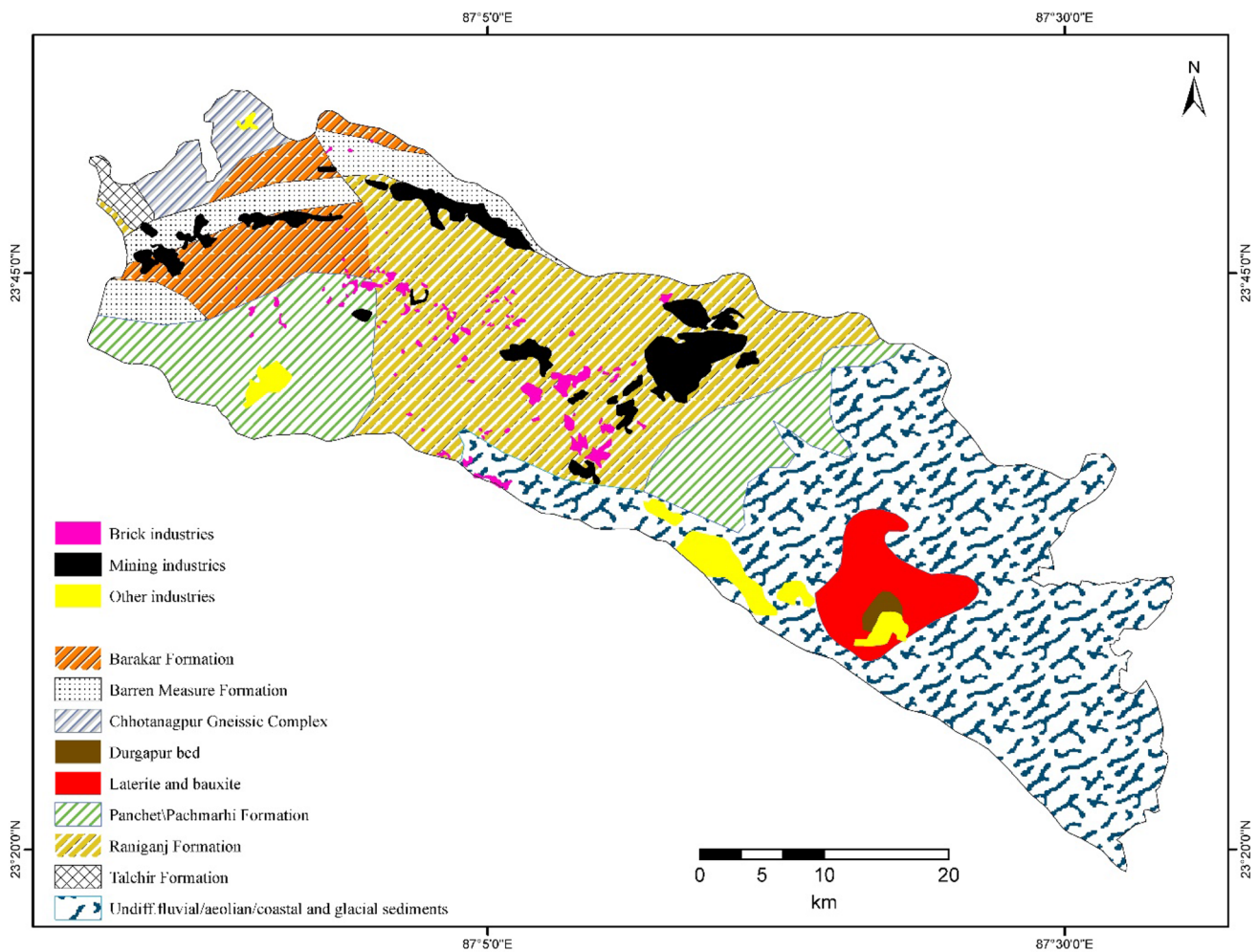


Fig. 2 Geology map of the study area

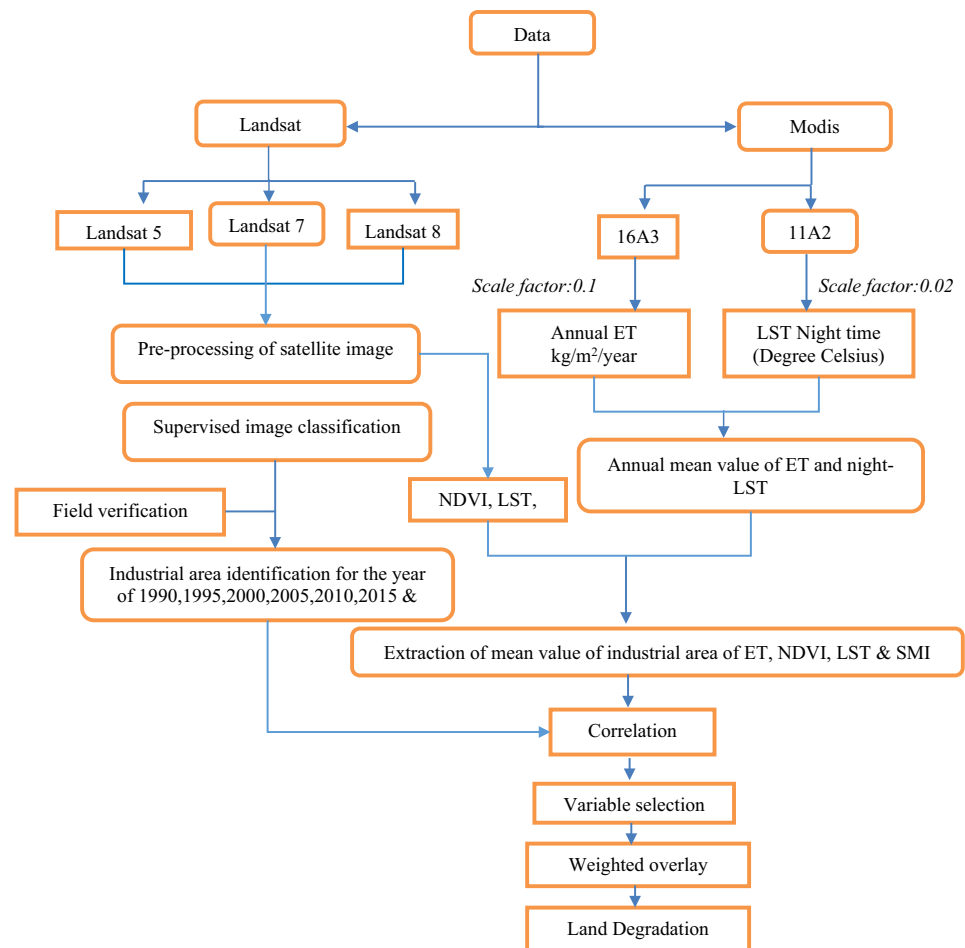
Table 1 Data used for the study

Sl. no.	Satellite name	Date of acquisition	Date of acquisition	Resolution (m)	Scale factor
1	Landsat-5	1/21/1990	4/11/1990	30	–
2	Landsat-5	1/19/1995	4/9/1995	30	–
3	Landsat-5	3/21/2000	3/29/2000	30	–
4	Landsat-5	2/15/2005	4/20/2005	30	–
5	Landsat-5	2/13/2010	4/2/2010	30	–
6	Landsat-8	3/15/2015	5/2/2015	30	–
7	Landsat-8	2/9/2020	5/15/2020	30	–
8	MODIS16A3	Yearly product (2000, 2005, 2010 and 2014)		500	0.1
9	MODIS11A2	Every 8-day data product (2000, 2005, 2010, 2015, 2020)		1000	0.02

image data is available from the years 2000 to 2014 (http://files.ntsg.umt.edu/data/NTSG_Products/MOD16/MOD16A3.105_MERRAGMAO/Geotiff/), we have used the data

for the years of 2000, 2005, 2010 and 2014. The metadata of the Landsat satellite and MODIS imageries are provided in Table 1.

Fig. 3 Methodology flowchart of the study



Industrial area classification

The major types of industries in the study area are mining industries, brick industries and other industries (Iron and steel, chemical, automobile and fertilizer industries, etc.). A supervised maximum likelihood image classification technique using ArcGIS 10.6 was used to extract the industrial regions from Landsat summer time imageries. Initially, training samples of 10 LULC categories such as waterbodies, tree cover, built-up, cropland, shrubland, grassland, bare/sparse vegetation, mining, brick and other industries were created. 50 training samples for each category of LULC were created to classify the image. From the classified raster image, a visual interpretation method was employed to remove the misclassified pixels. For example, pixels which were classified as water within the mining area were reclassified as mining area and in the similar way agricultural land and scrub land occurring within the brick industrial area were reclassified to the brick industrial area. All industrial clusters were cross verified with Google Earth images and ground truth verification. For the accuracy assessment of all LULC categories user's, producer's and overall accuracy were calculated using an error matrix table (Story and Congalton 1986).

The area under each industry is calculated discretely at a 5-year interval. The industrial area is computed in every 5 years in the analysis and the area of expansion of the industrial area every 5 years for each industry were calculated distinctly. In addition to that, the yearly industrial expansion rate has been evaluated by an average expansion rate given below by Seto et al. (2011):

$$100 \times \left(\left(\frac{IA_{2020}}{IA_{1990}} \right)^{\frac{1}{D}} - 1 \right), \quad (1)$$

where IA_{2020} and IA_{1990} are the area under a specific industry in 2020 and 1990, respectively, and D is the time interval in years.

Processing of satellite imageries

We examined the most commonly used land degradation indicators, daytime and night-time LST, NDVI, ET and SMI. LST for summer and winter, SMI and NDVI were derived for the study area and extracted for each industrial region separately at the 5-year equal interval, while MODIS imageries were utilized for seasonal night time LST and yearly

ET based on the availability of the satellite images. As we calculated industrial area at every 5-year interval, the same time interval was also followed for other land degradation indicators calculation as well. NDVI, SMI and seasonal LST were calculated for the years 1990, 1995, 2000, 2005, 2010, 2015 and 2020 with a spatial resolution of 30 m. Seasonal night-time LST was computed for the years 2000, 2005, 2010, 2015 and 2020, while yearly ET was derived for 2000, 2005, 2010 and 2014 years, respectively, as after 2014 MODIS16A3 data of ET is not available.

Satellite data is the only possible way of measuring LST over an extensive area with high and temporal resolution with more accurate information (Li et al. 2013). In this study, thermal remote sensing was used to capture changes in the energy balance of different surfaces in the Earth (Voogt and Oke 2003). The thermal bands of Landsat allow for estimation of LST (Anderson et al. 2012). LST derived from satellite provides an understanding of the urbanization patterns in the city (Walawender et al. 2014) as well as helps in the delineation of Urban Heat Island (UHI) (Liu et al. 2016; Fu and Weng 2016; Majkowska et al. 2017) in addition to assessing environmental change (He et al. 2017; Alvarez-Mendoza et al. 2019). The formula used for deriving LST (Artis and Carnahan 1982) from Landsat is given below:

$$LST = \frac{BT}{\left\{ 1 + \left[\left(\frac{\lambda BT}{\rho} \right) \ln \epsilon_{\lambda} \right] \right\}}, \quad (2)$$

where LST is the LST in °C (degree Celsius) Celsius, BT is the sensor brightness temperature in °C, λ is the emitted radiance wavelength, ϵ_{λ} represents land surface emissivity, and ρ is calculated using Boltzmann constant (k), the velocity of light (c) and Planck's constant (h).

Soil moisture derived from Landsat TM can be qualitatively assessed using Thermal Infra-Red (Thermal-IR) as there is an inverse relationship among them (Shih and Jordan 1993). Soil moisture retrieved from satellite image has applications in agricultural drought assessment (Hunt et al. 2009; Saha et al. 2018; Souto et al. 2019) and irrigation control (Mohamed et al. 2019). The lower and upper limits of LST are considered for calculating SMI (Moawad 2012) with the raster calculator tool using the equation given below:

$$SMI = \frac{LST_{\max} - LST}{LST_{\max} - LST_{\min}} \quad (3)$$

where LST_{\max} and LST_{\min} are the maximum value and minimum value of LST retrieved, while LST refers to the corresponding pixel LST.

NDVI is used as an indicator of the vegetative cover. The minimum value of NDVI is -1 which can go on increasing and have a maximum value of $+1$. The positive values of NDVI represent the increasing density of vegetation with 0

value as no vegetation and negative values represent non-vegetated surfaces, such as water or snow (Silleos et al. 2006). The water bodies and the nonappearance of vegetation will have NDVI values in the range of -1 to 0. NDVI is derived using Landsat imageries with the help of Red and Near Infra-red bands. NDVI is used to quantify the density and intensity of vegetation (Duarte et al. 2018; Mohajane et al. 2017; Fensholt et al. 2004) for classifying LULC. This spectral index can also be utilized to assess the quality of the environment (Fung and Siu 2000) and correlate with climatic factors (Song and Ma 2011; Matchanov et al. 2016; Zhang et al. 2016). The formula for computing NDVI (Rouse et al. 1974) is given in the following equation:

$$NDVI = \frac{NIR - RED}{NIR + RED} \quad (4)$$

where NIR and RED are the reflectance values of RED and Near Infra-Red (NIR) band of Multi-Spectral Sensor (MSS) of Landsat, respectively. The absence of vegetation or waterbody is represented by negative values. On the contrary, positive values denote vegetation with values above 0.5 representing dense vegetation.

To derive night-time LST from the MODIS 11A2 data product, we have multiplied each pixel value by the scale factor of 0.02 to get the LST value in Kelvin and finally converted it to °C (degree Celsius) by deducting 273.15. The same procedure was adopted for estimating ET from the MODIS16A3 product by multiplying the scale factor of 0.1 to get the ET value $\text{kg/m}^2/\text{year}$ (Das et al. 2020; Liu et al. 2019).

The mean NDVI value of each year for each industrial category (mining, brick and other industries) was calculated by overlaying and extracting raster NDVI value by the polygons of the respective industries and thus computed mean NDVI through the raster statistics tool available in ArcGIS 10.6. Similarly mean LST, ET, SMI were calculated. With the help of remote sensing spectral indices extracted, a correlation analysis is carried out to determine whether there is any relation between the expansion of industries and the mean spectral index value. From the above analysis, we will be able to arrive at the most critical indices contributing towards land degradation and the relation with industrial expansion.

Results and analysis

Landuse/land cover extent

Accuracy assessments of the classified LULC were carried out by computing users' and producers' accuracy of each land-use category. 50 ground truth verification points under each LULC category were taken to calculate the user's

and producer's accuracy of the LULC classification. Since our study area is mixed with the rural, urban and industrial region, more diverse land use categories within a small land parcel were observed and thus some of the pixels were misclassified. For example, mining areas were misclassified as waterbodies, some of the brick industrial areas were misclassified as bare or sparsely vegetated areas, also some of the cropland areas were misclassified as tree cover and grassland areas and viceversa. These misclassified pixels were reclassified to improve the LULC accuracy based on field visit and google earth images. Results show an overall accuracy of around 90.98% and the user's accuracy of brick, mining and other industries were 92%, 96% and 94% with the producer's accuracy 90%, 92% and 100%, respectively. Whereas, the user's accuracy of built-up, tree cover, cropland, grassland, bare/sparse vegetation, shrubland and waterbodies were 90%, 92%, 90%, 86%, 88%, 84% and 98% with the producer's accuracy of 93.75%, 92%, 88.2%, 86%, 83%, 89% and 96%, respectively. LULC for the year 2020 was computed and areal extent was calculated. Of the total study area cropland covers 49% followed by tree cover (19%), built-up (8%), bare or sparse vegetation (7%), grassland (6%), mining

(4%), other industries (3%), waterbodies (2%), brick industries (1%) and shrubland (1%), respectively (Fig. 4). Since our focus is on industrial regions, such as mining, brick and other industries, we only considered industrial regions for further analysis.

Growth in the industrial area over three decades

The spatial and temporal variation of the various industries in the West Burdwan district is shown in Fig. 5. The total area under industries has increased from 37.62 km² (2.06% area of the district) to 138.6 km² (7.61%) in the period from 1990 to 2020 and this increase is highly concentrated in the northwest and central regions of the district. The other industries occupied 37.45% of all industrial areas in the district in 1990. From that scenario, the district changed to a mining industrial area predominantly (occupying 51.96%) in 2020. The industrial clusters seen in 1990 only has expanded in successive three decades, while the northeastern and eastern region is mainly occupied by forest area, agricultural land and devoid of industries. The area under the various

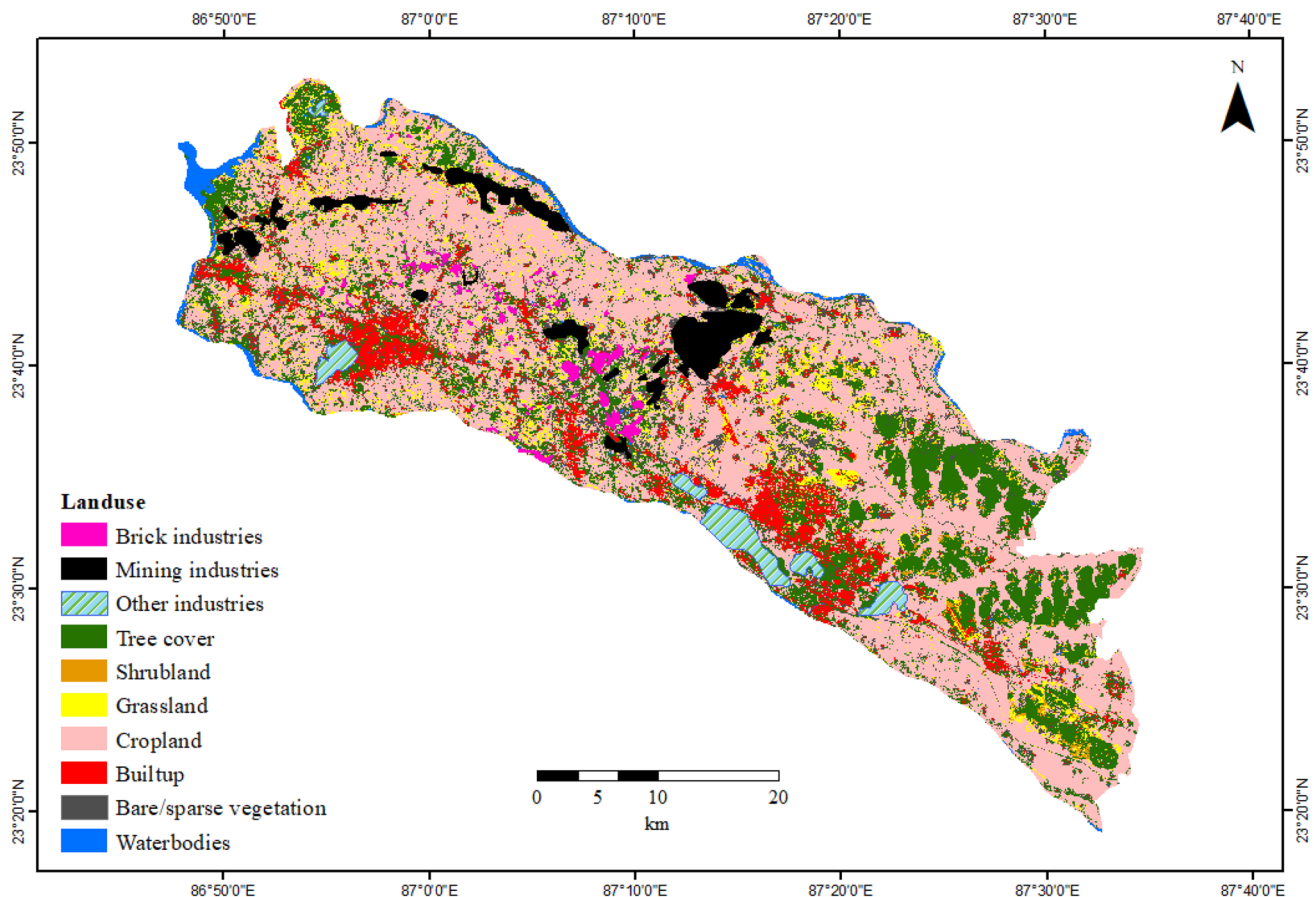


Fig. 4 Landuse of Paschim Burdwan

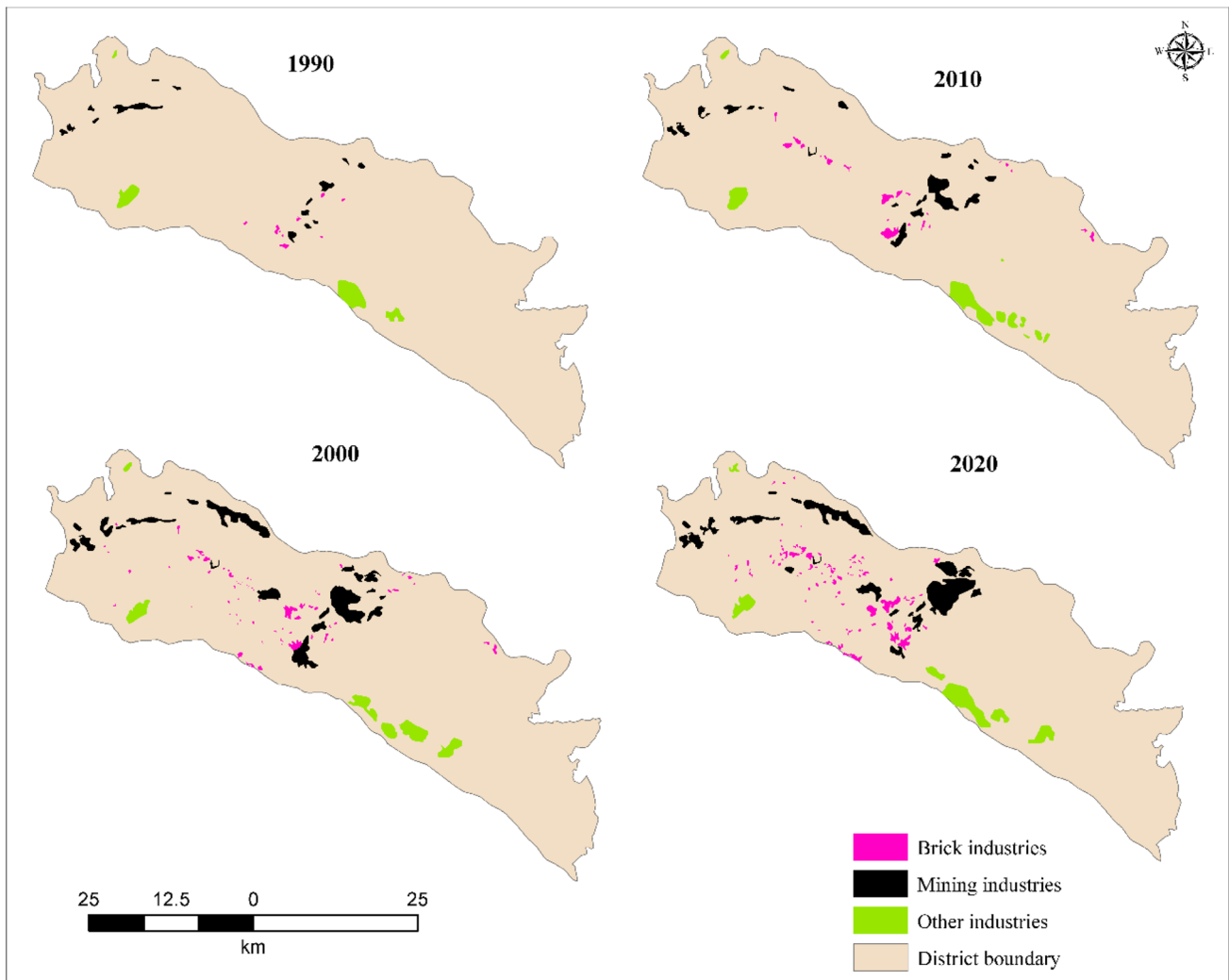


Fig. 5 Spatio-temporal variation of industries in West Burdwan district

industries and their expansion in the period of study from 1990 to 2020 is represented graphically in Fig. 6.

The coal mining area increased from 14.09 km² (37.45% of the total industrial area) in 1990 to 72.02 km² (51.96%) in 2020. The average rate of expansion was a maximum of 14.36% for 5 years from 1995 to 2000 followed by 7.36% and 4.25% for the successive 5-year periods. In the decade from 2010 to 2020, the average rate of expansion slowed down further (3.55% and 2.50%). Initially, the other industries were developed along the Damodar river and only those

have expanded in the period considered in this study. The area occupied by other industries had an average rate of expansion of 2.43% for the 5 years with a peak of 6.56% during the period from 2010 to 2015. The brick industries occupied only 2.14 km² (5.68% of the industrial area) in 1990. The central and western region is dotted with scattered brick industries contributing to 16.30% of the industrial area in 2020 mainly due to the peak average rate of expansion of 26.76% observed between 1995 to 2000.

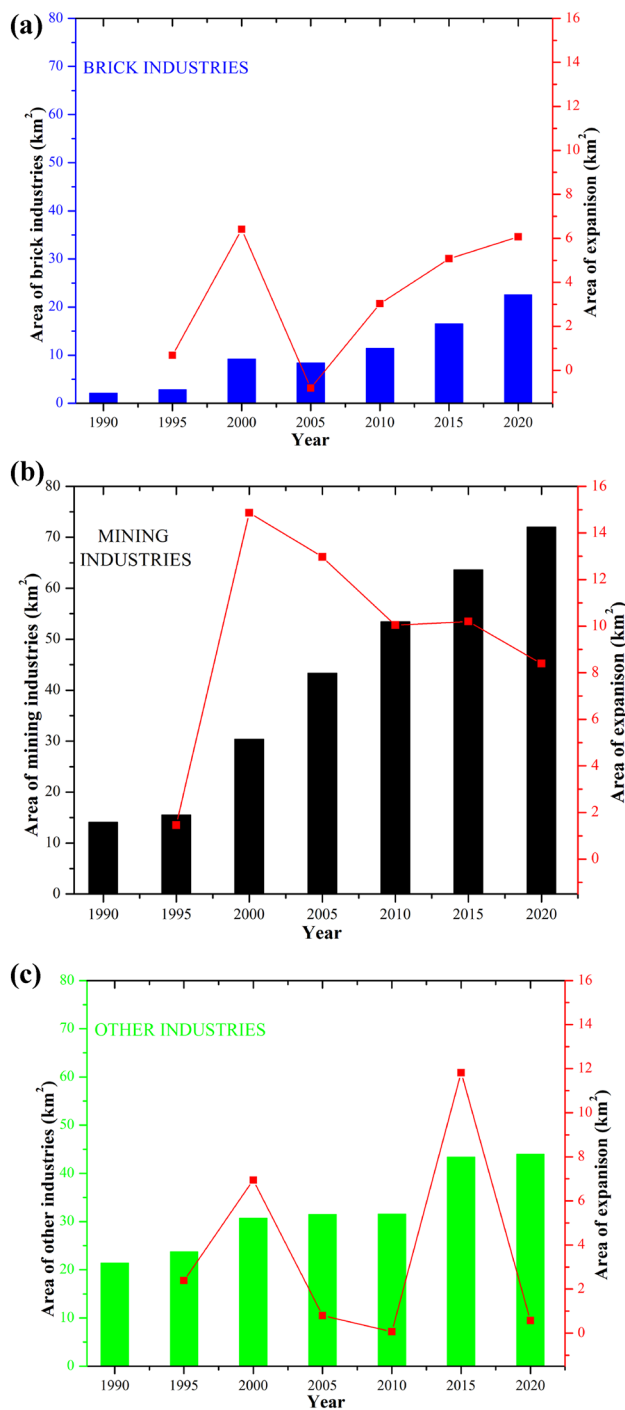


Fig. 6 a Area under brick and the corresponding area of expansion, b other industries and the corresponding area of expansion, c mining industries and the corresponding area of expansion

Variation of satellite-derived environmental indices

Normalized Difference Vegetation Index (NDVI)

The minimum NDVI values in the mining industrial area decreased from -0.135 to -0.2 over three decades with a continuous decline except in 2005. The mean values reduced by 69.27% (from 0.192 to 0.059) over 30 years suggesting the vegetation cover in the mining area has reduced. This decreasing NDVI value is a sign of vegetation degradation but we have to take into account that water stored up in these areas during mining activities also. The decreasing trend of NDVI is also evident in other industrial areas with a continuous decline of maximum NDVI values from 0.75 in 1990 to 0.59 in 2015. The mean NDVI value also decreased from 0.213 in 1990 to 0.116 in 2020, a reduction of 45.53%. Concerning the brick industries, the mean NDVI values reduced from 0.179 to 0.102, a drop of almost 30% (29.05%). No such trend can be ascertained for the maximum and minimum NDVI values for brick industries.

The negative values of the average annual change of NDVI from 1990 to 2020 are shown in Fig. 7. The average annual rate of decreasing NDVI values covers 166.34 km² (9.15% of the study area). The total area under mining industries in 2020 is 3.96% of the study area and it contributes to 19% of an average annual rate of decreasing NDVI values, while brick and other industries with 1.24% and 2.42% of the area contribute to 5% of the decreasing values each. More than 40% of the mining industrial and brick industrial areas, have an average annual rate of decreasing NDVI. The total industrial area under the district in 2020 was 7.62% and it contributes to 29.73% of the decreasing NDVI values. The southern region of the district which shows high negative values is because of the non-cultivation during the time of imagery. This area has been cultivated in all the years of analysis from 1990 to 2015 with high positive values of NDVI above 0.6. Cultivation has taken place during 2019 also and has not taken place during 2020 and this cannot be considered as land degradation.

Land Surface Temperature (LST)

The summer daytime average LST values increased over mining industrial region by 13.94% (32.65–37.20 °C) in the study period. The range of the mean values for both mining and other industries is around 6.3 °C (32.5–39 °C), whereas for brick industries were slightly higher at 8.34 °C.

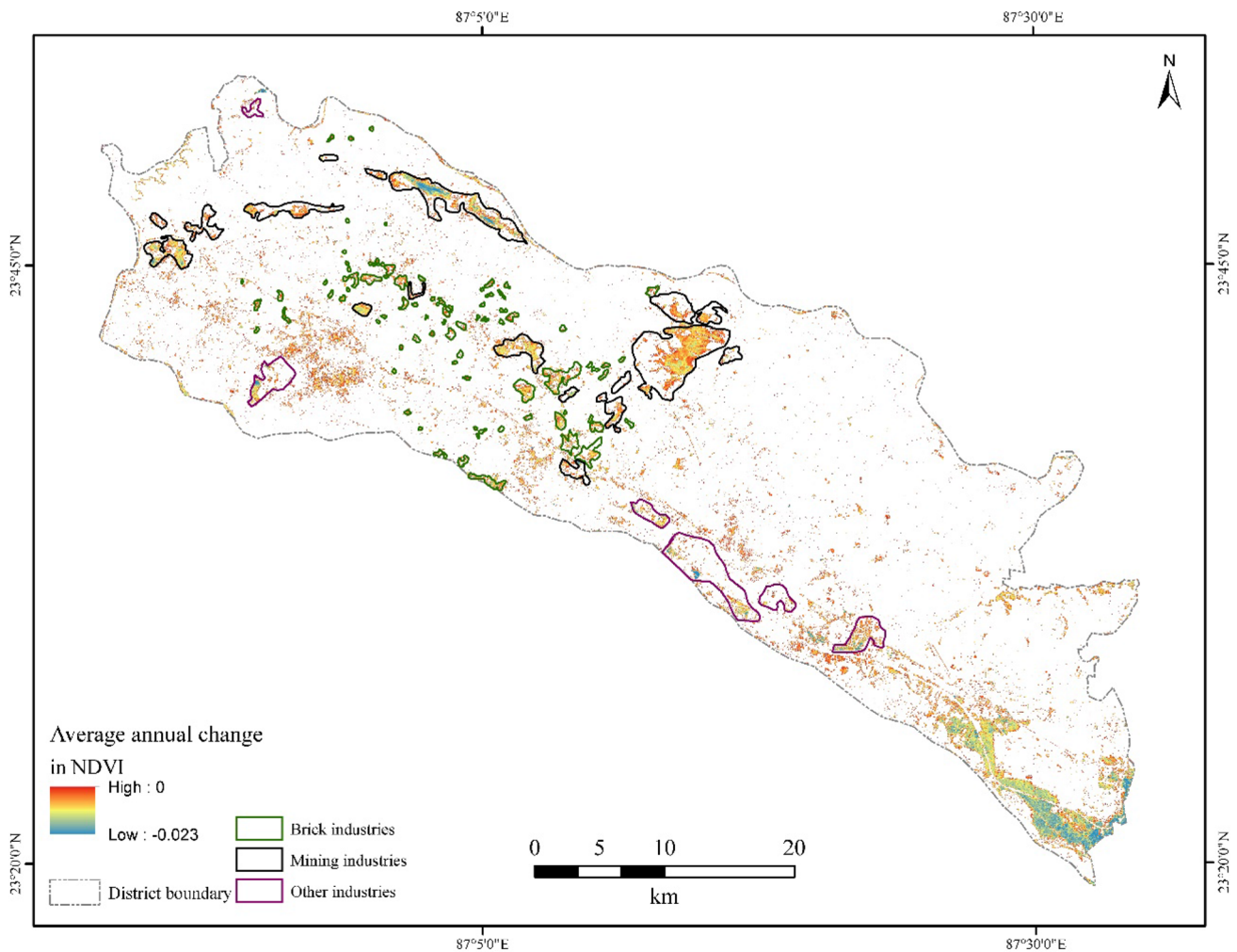


Fig. 7 Annual average rate of change of NDVI between 1990 and 2020 showing decreasing values

For mining industries, the minimum LST range was 4.78 °C (22–27.10 °C), while for brick (12.7 °C) and other industries (13.49 °C), it was higher than 10 °C. The average annual increasing rate of LST for summer daytime was represented in Fig. 8. 38.54% of the West Burdwan district was found to be an increase in annual average LST values. Out of the 72.02 km² of mining area in 2020, 34.05 km² (47.28%) area contribute to 5% (4.86%) of the total area under the district having an average annual increasing rate. 8.67 km² area (38.38%) of brick industries and 10.52 km² (23.92%) of other industries also contribute to the annual average increase in LST rate. The total industrial area under the district contributes to 7.59% of the area with the annual average increasing rate of summer daytime LST. There was no increasing or decreasing trend observed in the summer night LST, winter daytime LST and winter night-time LST. As a result, they have not been considered for further investigation.

Evapotranspiration (ET)

The variation of ET was calculated from the MODIS16A3 data. The declining ET values was the general trend observed for all the industries except for the maximum yearly values in the 14 years. The mean values of ET for mining, brick and other industries decreased continuously by 17.00%, 190.9% and 28.15%, respectively, in the period from 2000 to 2014. The decreasing trend was also observed in the minimum ET values. The minimum values for all industries ranged between 550 and 425 kg/m²/year in the 14 years with the other industries recorded highest fall of 26.73% followed by brick (20.61%) and mining (18.18%) industries. The decreasing trend in ET may be due to the degradation of vegetation and increasing industrial area which also supports the decrease in NDVI trend in respective years.

The average annual decrease of ET values is shown in Fig. 9. Around 65% of the West Burdwan district observed decreasing ET values. The brick industrial area had 77.17%

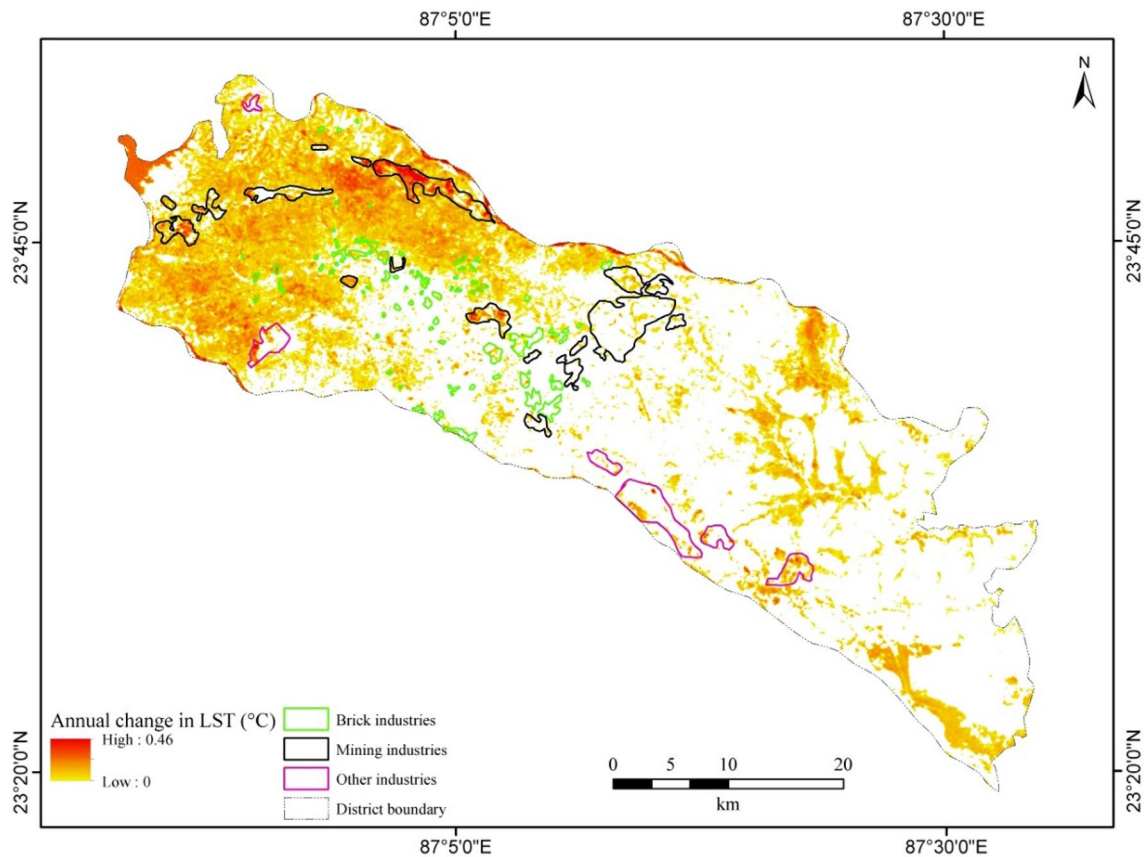


Fig. 8 Annual average rate of change of summer daytime LST values between 1990 and 2020 showing increasing values

(12.75 km²) of its area with decreasing values, whereas other industries had 34.86% (15.14 km²) with the highest average annual mean decreasing rate of -8.73 kg/m²/year. On the whole, the entire industrial area (123.57 km²) 6.79% of the district contributes to 6.01% of the area with decreasing ET rate.

Soil Moisture Index (SMI)

SMI derived from Landsat imageries starting from 1990 has a range from 0 to 1. SMI values 0 to 0.1 refer to severe drought, 0.1 to 0.2 moderate drought, 0.2 to 0.3 slight drought and above 0.3 value represents no drought condition (Parida et al. 2004). The maximum and mean values of SMI is showing an increasing trend for all three industries during the study period. In 1990, the mean value of SMI was around 0.43 for all industries and it increased to 0.672 (56.27%) for mining, 0.691 (62.97%) for brick and 0.72 (66.05%) for other industries in 2020. The mean SMI value shows a positive correlation with increasing mining and brick areas with adjusted R^2 values of 0.572 and 0.658, respectively (p value

less than 0.05). The increasing trend of SMI values is not considered for further analysis.

Correlation between growth in the industrial area and satellite-based environmental indices

NDVI, summer daytime LST, and ET had significant correlation (adjusted $R^2 > 0.5$ and $p < 0.05$) with the increase mining area. The other industrial and brick industrial areas indicate an insignificant correlation with environmental indices and those values were not reported. The vegetation index and ET had a negative correlation with the increasing mining area, whereas the temperature had a positive correlation, as represented in Fig. 10. The area under land degradation is calculated and tabulated along with the mean decreasing/increasing values in Table 2.

Mean NDVI values were calculated by extracting each year NDVI raster value by the same year industrial area polygon through spatial statistics tool in ArcGIS 10.6 and thus calculated each raster average value through raster statistic. The correlation result between the mean NDVI value and the increased mining industry area shows a negative relationship with the adjusted R^2 value of 0.57 and

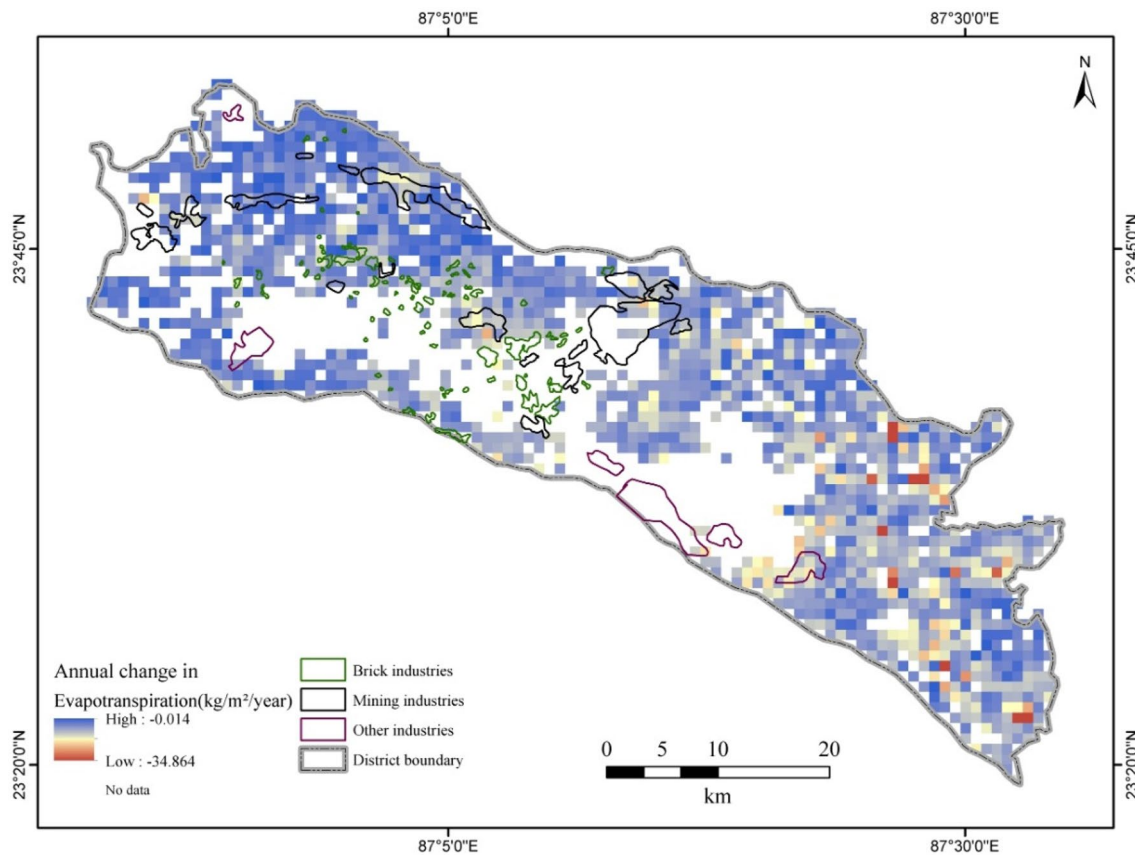


Fig. 9 Annual average rate of change of Evapotranspiration values between 2000 and 2014 showing increasing values

p value of 0.029. As the mining area increases, the NDVI values decrease due to various factors, such as changes in land use, decaying vegetation, etc. The mean decreasing rate of NDVI for the mining area is 7.89% higher when compared to the entire West Burdwan district.

The positive correlation between mean summer daytime LST and mining area is due to the change in land cover of the area and mining activity. With an Adjusted R^2 of 0.51 at 95% level of significance ($p = 0.04$). Nearly 50% (47.27%) of the mining area has a mean increasing rate of LST in the summer daytime with 25.80% increased mean value ($+0.39$ °C) when compared to the overall district value ($+0.31$ °C).

The negative correlation between mining industrial area and ET was very high (Adjusted $R^2 = 0.949$). The relation was highly significant with a p value of 0.0168. The increase in the mining area of 51.94% (30.42 km² in 2000 to 63.63 km² in 2014) has resulted in 67.65% of the mining area in 2014 having annual average decreasing ET values. The mean decreasing value of ET for mining industries is -6.44 (kg/m²/year) which is 12.11% lower than the entire district value.

Discussion

Observed areas under land degradation in West Burdwan district

The analyses of land degradation indicators examined in the present study demonstrate that the West Burdwan district is experiencing land degradation in terms of the degrading vegetation cover, decreasing ET and hotter local climate over the last 30 years based on the analyzed data. The magnitude of land degradation is more severe in the north, central and northwestern regions, where coal mines are located. However, the study did not detect enough changes in soil moisture and night-time LST over the study period. This result could indicate that MODIS coarse resolution may not be appropriate enough to the West Burdwan district, where natural and manmade land classes are sparsely distributed.

Over the years, the spatial concentration of industries in the north and central regions of the district only increased due to various reasons. The mining industries are concentrated in the north-western and central regions of the district (coinciding with geology), whereas the other industries are agglomerated towards the south-eastern region mainly

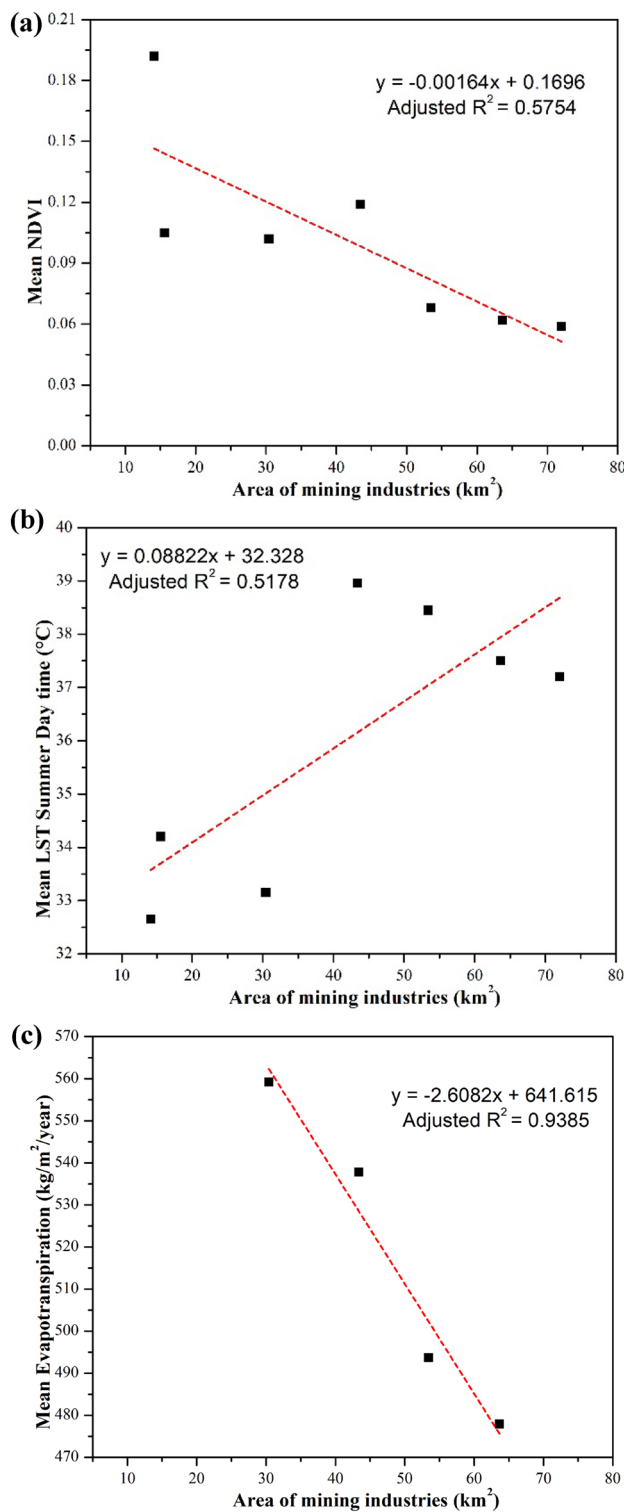


Fig. 10 **a** Relationship between area of mining industries and NDVI, **b** mining industries and LST summer daytime, and **c** mining industries and evapotranspiration

due to transport connectivity and water source. The brick industries are scattered throughout the central and western regions of the district. A highly skewed distribution of industries towards the northwest and central regions of the West Burdwan district was also observed. The area affected by land degradation also coincides with the areas of industrial development with 7.62% of the area under the district contributing to 29.7%, 7.59% and 6.01% degradation area of NDVI, summer daytime LST and ET, respectively. The proper clustering of industries in the northern region of the district would have lessened the effect of land degradation.

Mining nearby regions are experiencing a quicker rate of land degradation as compared to the other places of the district. More than 40% of the mining area were experiencing degradation for all the land degradation indices (day and night LST, ET, NDVI and SMI). The non-mining area in 1990 such as forests (20.20%) and agriculture (79.79%) has changed to a mining area of 57.93 km² over the three decades and this has contributed to the 31.62 km² area of decreasing NDVI values which finally increased the summer daytime LST and also decrease annual ET rate. With the industrial area increase, the average NDVI value decreases simultaneously which represents the vegetation destruction in the industrial area. Several studies suggested that changes in human practices (e.g., land use) can significantly affect NDVI (Neigh et al. 2008; Mueller et al. 2014). Mining areas were found to be increasingly warmer with decaying vegetation resulting in the creation of hotspots surrounding the mining areas mainly due to the increase in mining activities and land-use change. Studies show that the highest LST has been noticed in industrial areas, especially in coal mining areas (Choudhury et al. 2019). Human interventions in the Earth caused the heterogeneity and complexity in the land surface characteristic recently which increases the variation in LST spatially (Yue et al. 2007; Zhang et al. 2009; Chi et al. 2015). Siddique et al. 2020 noticed that rapid changes in LULC in Asansol City from 2000 to 2018 was mainly due to built-up and industrial area which includes mining and quarries. As the mining progresses, the mine dump area increases. The increase in the maximum NDVI value in 2020 (from 0.52 in 2015 to 0.72 in 2020) is due to the growth of vegetation over mine dump after a certain period and this is visible in the degradation map with no increasing LST values over the same area which contributes to the land reclamation process and cannot be considered as land degradation (Kumar et al. 2015). The increase in SMI in mining areas is mainly because of the deposition of underground water in the mining areas due to the extraction of minerals. However, the increase in soil moisture is not an indicator of land degradation, but the deposition of underground water over the mining pond creates instability in the pit slopes which may create landslides in the mining regions (Loupasakis 2020).

Table 2 Land degradation area under various indices and their mean degradation rate

Area under consideration	Indices					
	NDVI		Summer daytime LST		Evapotranspiration	
	Area (km ²)	Mean decreasing rate (NDVI/year)	Area (km ²)	Mean increasing LST rate (°C)	Area (km ²)	Mean ET decreasing rate (kg/m ² /year)
West Burdwan district	166.34	-0.0038	700.53	+0.31	1180	-5.923
Mining industries	31.62	-0.0041	34.05	+0.39	43.03	-6.44
Brick industries	9.34	-0.0020	8.67	+0.34	12.75	-6.5
Other industries	8.48	-0.0045	10.52	+0.21	15.14	-8.73

More than 50% of the West Burdwan district shows decrease ET values. Vegetation degradation and declined ET, finally contribute to increasing LST which is one of the major factors that control the physical and organic cycles at the interface between the Earth and climate and highly affect the vegetation condition and soil water (Owen et al. 1998; Zhang et al. 2009; Li et al. 2018; Urqueta et al. 2018). It is very challenging to demarcate exact land degradation areas. To exactly demarcate the areas under land degradation, high-resolution imageries are much required to provide better accuracy. The use of coarser-resolution MODIS imageries (500 m) for ET reduces the accuracy level.

Mining industries showed a significant correlation with all the land degradation indicators (NDVI, LST, ET and SMI), whereas the same cannot be considered about the increase in brick and other industrial areas. From Table 2, it is evident that a considerable portion of the total industrial area is contributing to land degradation, although statistically, it is insignificant. Hence, the effect of brick and other industries also needs to be discussed in land degradation.

The other industries have the highest rates of decreasing mean NDVI and mean ET. As a result, there is high intensity of land degradation in the other industrial area, concentrated in a few pockets within its premises. However, the annual ET and soil moisture indices are not considered in the analysis, because the other industries are made of concrete or steel structures, absence of soil and vegetation cover. The other industries have the least increasing rates of LST. This is maybe due to the less annual expansion rate of industries and the geographical location, i.e., proximity to perennial Damodar river as well as surrounded by agricultural areas.

With regards to the summer daytime LST, the north-western region of the district with scattered brick industries and mining areas causes an increase in the annual average LST rates (Choudhury et al. 2019). The maximum temperature observed over the industrial regions, especially over the coal mining areas (Choudhury et al. 2019). The brick industries contribute to the increase in LST due to the burning of mud to make bricks and areas devoid of vegetation. The decrease

Table 3 Weightage to standardized indicators under different scenarios

Scenarios	Parameters		
	Standardized NDVI (%)	Standardized LST (%)	Standardized ET (%)
Scenario A	33	33	33
Scenario B	50	25	25
Scenario C	25	50	25
Scenario D	25	25	50

in SMI is mainly due to the increase in brick industrial areas and the degradation of vegetation.

The eastern and southern regions of the district are covered by forests and agricultural areas with very few villages. Noticeable changes in land use were not observed in these areas as compared to the mining region. Very few patches in the forest side of the district were showing average annual decreasing NDVI values and increasing LST values with less intensity. Sparse vegetation in the forests and agricultural area shows decreasing ET values. Although the geographical nature of the West Burdwan district favoured the commencement of industries and its growth when compared to its neighbouring districts, proper land planning and management were not practised leading to widespread land degradation in the industrial core of the district.

Scenarios of land degradation index

To provide overall land degradation in the study area, we have used the land degradation index (LDI), which is a weighted combination of changes in land degradation indicators considered in the present study. All the pixels of NDVI, LST and ET undergoing negative change of land degradation are standardized separately from 0 (no change) to 1 (high rate of change), which refers to changes from relatively slow to fast. The standardized indicators are then weighted and added together to produce an LDI with a valid

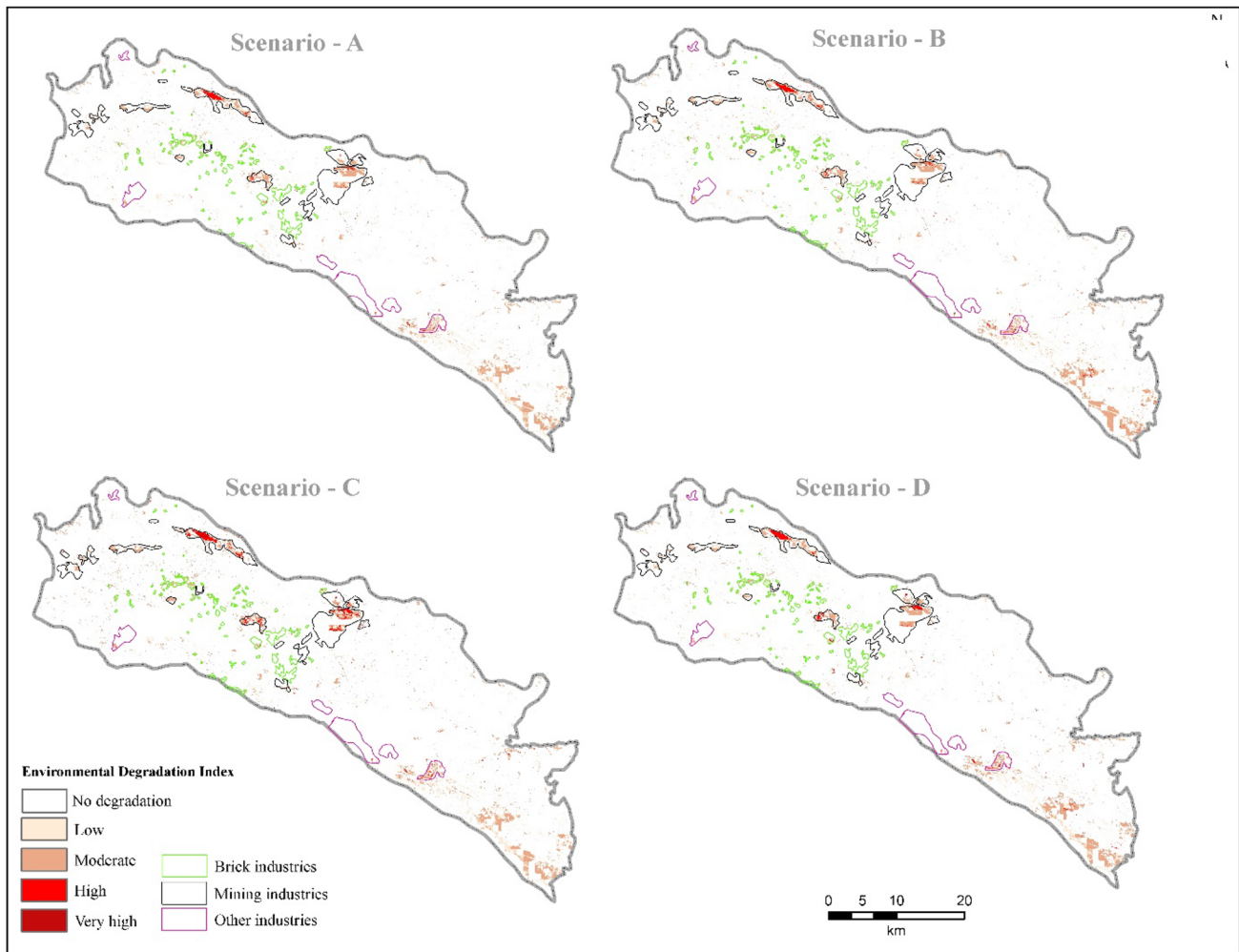


Fig. 11 Land degradation scenarios

range of 0 to 1. The standardized each indicator was than reclassified into 5 classes 0 (no change) to 0.2 (very low degradation), 0.2 to 0.4 (low degradation), 0.4 to 0.6 (moderate degradation), 0.6 to 0.8 (high degradation) and 0.8 to 1.0 (very high degradation), respectively (Hossain et al. 2020). Four different scenarios are considered by assigning different weights to each standardized index value (Table 3) and overlay analysis performed to calculate Land Degradation Index (valid range from 0 to 1) for each distinct scenario. The area under the varying intensity of land degradation for each scenario was computed. From the scenario analysis, it is found that Scenario C is the worst-case scenario because of the higher area under the increased intensity of land degradation as compared to others (Category 3 and Category 4). Scenario A with equal weightage to all the parameters yields the best-case scenario (Fig. 11). The area under the district undergoing cumulative land degradation due to increasing LST, decreasing NDVI and decreasing ET is 91.01 km². The

contribution of the total industrial area (7.62%) to the land degradation under the district is 30.2% (27.15 km²).

Most of the study region shows no degradation to low degradation. However, moderate-to-very high degradation was found over the mining industrial regions. Brick and other industrial regions show moderate to low degradation over the study area. Therefore, we suggest that areas of moderate to very high degradation may require more attention from local decision-makers and environmental inspectors.

Conclusions

Within the present work, we assessed land degraded areas in West Burdwan district, West Bengal using different land degradation indicators such as NDVI, ET, LST day and night, SMI through Landsat and MODIS satellite images from the years 1990–2020 at every 5-year interval. Results indicate that the growing trend of industries negatively influences

the land degradation indicators, such as NDVI, daytime LST and ET. Our findings confirmed that industrial growth influences the land degradation indicators such as decreasing the NDVI and ET values increases LST values in the industrial growing regions and surrounding areas. The overall result shows moderate to the very high level of land degradation observed over the industrial (mining, brick and other industries) regions, whereas most of the region shows very less to no changes in the land degradation indicators. Continuous expansion of industries highly concentrated in one particular area is observed to be one of the serious environmental stressors. Other possible stressors, such as increasing population are not included in the investigation, which may also have some effects to the local environment. To manage future industrial expansion, policymakers need to focus on de-clustering of industries throughout the district so that areas experiencing increasing LST, decreasing NDVI, and decreasing ET areas are considerably reduced. This analysis of industrial expansion and land degradation will help decision-makers, environmental regulators to provide better management practices for a sustainable future.

Different indicators of land degradation such as NDVI, LST, and SMI were evaluated from Landsat satellite of 30 m spatial resolution which is not enough to classify different small industries, may overestimate the areal extent. High-resolution satellite imagery such as Sentinel-2 satellite imagery of 10-m spatial resolution has the potential to get better output for different large and small scale industry mapping. However, in this study, we have cross-validated our images classification with Google Earth high-resolution images to avoid the classification error. Other indicators such as ET, night LST were computed from MODIS satellite of 500 and 1000 m spatial resolution. The use of high-resolution satellite data provides the potential for the generation of more accurate land degradation areas at the desired scale. However, the present study provides a basic idea about land degraded areas over the West Burdwan district which may help the environment planners for the betterment of the degraded land areas in future.

Acknowledgements The authors would like to acknowledge the Department of Civil Engineering, Anna University for facilitating the research work.

Author contributions SK: Conceptualization, Investigation and Methodology, Validation; ED: Writing - original draft preparation; MR: Writing - review & editing.

Funding This study did not receive any external funding.

Data availability All data sets generated for this study are included in the manuscript and the satellite data is available in the USGS website (<https://earthexplorer.usgs.gov/>).

Declarations

Conflict of interest There is no conflict of interest between the authors. All the authors have read and accepted the final version of the manuscript.

References

- Abd El-Hamid HT, Caiyong W, Hafiz MA, Mustafa EK (2020) Effects of land use/land cover and climatic change on the ecosystem of North Ningxia. *China Arab J Geosci* 13:1099. <https://doi.org/10.1007/s12517-020-06047-6>
- Abu Hammad A, Tumeizi A (2012) Land degradation: socioeconomic and environmental causes and consequences in the eastern Mediterranean. *Land Degrad Dev* 23(3):216–226. <https://doi.org/10.1002/ldr.1069>
- Adamo SB, Crews-Meyer KA (2006) Aridity and desertification: exploring environmental hazards in Jáchal, Argentina. *Appl Geogr* 26(1):61–85. <https://doi.org/10.1016/j.apgeog.2005.09.001>
- Alvarez-Mendoza CI, Teodoro A, Ramirez-Cando L (2019) Spatial estimation of surface ozone concentrations in Quito Ecuador with remote sensing data, air pollution measurements and meteorological variables. *Environ Monit Assess* 191(3):1–15. <https://doi.org/10.1007/s10661-019-7286-6>
- Anderson MC, Allen RG, Morse A, Kustas WP (2012) Use of Landsat thermal imagery in monitoring evapotranspiration and managing water resources. *Remote Sens Environ* 122:50–65. <https://doi.org/10.1016/j.rse.2011.08.025>
- Artis DA, Carnahan WH (1982) Survey of emissivity variability in thermography of urban areas. *Remote Sens Environ* 12:313–329. [https://doi.org/10.1016/0034-4257\(82\)90043-8](https://doi.org/10.1016/0034-4257(82)90043-8)
- Bai Z, Dent D, Olsson L, Schaepman M (2008) Proxy global assessment of land degradation. *Soil Use Manag* 24:223–234. <https://doi.org/10.1111/j.1475-2743.2008.00169.x>
- Boer MM (1999) Assessment of dryland degradation: linkage theory and practice through site water balance modeling. Ph.D. Thesis, Faculteit Ruimtelijke Wetenschappen Universiteit Utrecht
- Cheung SY, Walker IJ, Myint SW, Dorn RI (2021) Assessing land degradation induced by recreational activities in the Algodones Dunes, California using MODIS satellite imagery. *J Arid Environ* 185:104334. <https://doi.org/10.1016/j.jaridenv.2020.104334>
- Chitade AZ, Katyar SK (2010) Impact analysis of open cast coal mines on land use/land cover using remote sensing and GIS technique: a case study. *Int J Eng Sci Technol* 2(12):7171–7176
- Chi Y, Shi H, Wang X, Feng A (2015) The spatial-temporal characteristics and impact factors of land surface temperature on Five Southern Islands of Miaodao Archipelago, Shandong, China. *Chin J Ecol* 34(8):2309–2319
- Choudhury D, Das K, Das A (2019) Assessment of land use land cover changes and its impact on variations of land surface temperature in Asansol-Durgapur Development Region. *Egypt J Remote Sens Space Sci* 22(2):203–218. <https://doi.org/10.1016/j.ejrs.2018.05.004>
- Das S (2020) Impact of brick industries on geo-environment alongside the Bhagirathi-Hugli River, West Bengal, India using statistical techniques and RS and GIS applications. *Int J Sci Res* 9(8):1266–1277
- Das P, Vamsi KS, Zhenke Z (2020) Decadal variation of the land surface temperature (LST) and Urban Heat Island (UHI) over Kolkata city projected using MODIS and ERA-Interim datasets. *Aerosol Sci Eng* 4:200–209. <https://doi.org/10.1007/s41810-020-00067-1>

- De Jong SM (1994) Applications of reflective remote sensing for land degradation studies in a Mediterranean environment. *Nederlandse geografische studies*, vol 177. Utrecht University, Utrecht
- De Jong R, De Bruin S, Schaepman M, Dent D (2011) Quantitative mapping of global land degradation using Earth observations. *Int J Remote Sens* 32(21):6823–6853. <https://doi.org/10.1080/0143161.2010.512946>
- D'Odorico P, Bhattachan A, Davis KF, Ravi S, Run-yan CW (2019) Global desertification: drivers and feedbacks. *Adv Water Resour* 51:326–344
- Duarte L, Teodoro AC, Monteiro AT, Cunha M, Gonçalves H (2018) QPhenoMetrics: an open source software application to assess vegetation phenology metrics. *Comput Electron Agric* 148:82–94. <https://doi.org/10.1016/j.compag.2018.03.007>
- Dutta S, Guchhait SK (2020) Assessment of land use land cover dynamics and urban growth of Kanksa Block in Paschim Bardhaman District, West Bengal. *Geo J* 13:1–20. <https://doi.org/10.1007/s10708-020-10292-3>
- Faour G (2014) Detection and mapping of long-term land degradation and desertification in arab region using MODERSAT. *Leban Sci J* 15(2):119–131
- Fensholt R, Sandholt I, Rasmussen MS (2004) Evaluation of MODIS LAI, fAPAR and the relation between fAPAR and NDVI in a semi-arid environment using in situ measurements. *Remote Sens Environ* 91(3–4):490–507. <https://doi.org/10.1016/j.rse.2004.04.009>
- Fu P, Weng Q (2016) Consistent land surface temperature data generation from irregularly spaced Landsat imagery. *Remote Sens Environ* 184:175–187. <https://doi.org/10.1016/j.rse.2016.06.019>
- Fung T, Siu W (2000) Environmental quality and its changes, an analysis using NDVI. *Int J Remote Sens* 21(5):1011–1024. <https://doi.org/10.1080/01431600210407>
- Gao J, Liu Y (2010) Determination of land degradation causes in Tongyu County, Northeast China via land cover change detection. *Int J Appl Earth Obs Geoinf* 12(1):9–16. <https://doi.org/10.1016/j.jag.2009.08.003>
- Ghorai D, Ziauddin G, Sarkar S, Singh M S, Chatterjee J, Ghatak S, Sinha G, Ghosh P (2018) Comprehensive district agriculture plan, Paschim Bardhaman for 2017–18 to 2019–20
- Gong JR, Wang Y, Liu M et al (2014) Effects of land use on soil respiration in the temperate steppe of Inner Mongolia, China. *Soil till Res* 144:20–31
- He C, Gao B, Huang Q, Ma Q, Dou Y (2017) Environmental degradation in the urban areas of China: evidence from multi-source remote sensing data. *Remote Sens Environ* 193:65–75. <https://doi.org/10.1016/j.rse.2017.02.027>
- Hein L, De Ridder N, Hiernaux P, Leemans R, De Wit A, Schaepman M (2011) Desertification in the Sahel: towards better accounting for ecosystem dynamics in the interpretation of remote sensing images. *J Arid Environ* 75:1164–1172. <https://doi.org/10.1016/j.jaridenv.2011.05.002>
- Higginbottom TP, Symeonakis E (2014) Assessing land degradation and desertification using vegetation index data: current frameworks and future directions. *Remote Sens* 6:9552–9575. <https://doi.org/10.3390/rs6109552>
- Hossain A, Krupnik TJ, Timsina J, Mahboob MG, Chaki AK, Farooq M, Bhatt R, Fahad S, Hasanuzzaman M (2020) Agricultural land degradation: processes and problems undermining future food security. In: *Environment, climate, plant and vegetation growth*. Springer, Cham, pp 17–61
- Hunt ED, Hubbard KG, Wilhite DA, Arkebauer TJ, Dutcher AL (2009) The development and evaluation of a soil moisture index. *Int J Climatol* 29(5):747–759. <https://doi.org/10.1002/joc.1749>
- ISRO (2016) Desertification and Land Degradation Atlas of India. https://www.sac.gov.in/SACSITE/Desertification_Atlas_2016_SAC_ISRO.pdf
- Joshi PK, Kumar M, Paliwal A, Midha N, Dash PP (2009) Assessing impact of industrialization in terms of LULC in a dry tropical region (Chhattisgarh), India using remote sensing data and GIS over a period of 30 years. *Environ Monit Assess* 149(1):371–376. <https://doi.org/10.1007/s10661-008-0211-z>
- Kumar S, Maiti SK, Chaudhuri S (2015) Soil development in 2–21 years old coalmine reclaimed spoil with trees: a case study from Sonepur-Bazari opencast project, Raniganj Coalfield, India. *Ecol Eng* 84:311–324. <https://doi.org/10.1016/j.ecoleng.2015.09.043>
- Lambin EF, Geist HJ, Lepers E (2003) Dynamics of land-use and land-cover change in tropical regions. *Annu Rev Environ Resour* 28:205–241. <https://doi.org/10.1146/annurev.energy.28.050302.105459>
- Lanorte A, Lasaponara R, Lovallo M, Telesca L (2014) Fisher–Shannon information plane analysis of SPOT/VEGETATION Normalized Difference Vegetation Index (NDVI) time series to characterize vegetation recovery after fire disturbance. *Int J Appl Earth Obs* 26:441–446. <https://doi.org/10.1016/j.jag.2013.05.008>
- Lasanta T, García-Ruiz JM, Pérez-Rontomé MC, Sancho-Marcén C (2000) Runoff and sediment yield in a semi-arid environment: the effect of land management after farmland abandonment. *CATENA* 38:265–278. [https://doi.org/10.1016/S0341-8162\(99\)00079-X](https://doi.org/10.1016/S0341-8162(99)00079-X)
- Li Z, Tang B, Wu H, Ren H, Yan G, Wan Z, Trigo F, Sobrino IA (2013) Satellite derived land surface temperature: current status and perspectives. *Remote Sens Environ* 131:14–37. <https://doi.org/10.1016/j.rse.2012.12.008>
- Li X, Zhou Y, Asrar GR, Zhu Z (2018) Creating a seamless 1 km resolution daily land surface temperature dataset for urban and surrounding areas in the conterminous United States. *Remote Sens Environ* 206:84–97. <https://doi.org/10.1016/j.rse.2017.12.010>
- Liu K, Su H, Li X, Wang W, Yang L, Liang H (2016) Quantifying spatial–temporal pattern of urban heat island in Beijing: an improved assessment using land surface temperature (LST) time series observations from LANDSAT, MODIS, and Chinese new satellite GaoFen-1. *IEEE J Select Top Appl Earth Obs Remote Sens* 9(5):2028–2042. <https://doi.org/10.1109/JSTARS.2015.2513598>
- Liu W, Agusdinata DB, Myint SW (2019) Spatiotemporal patterns of lithium mining and environmental degradation in the Atacama Salt Flat, Chile. *Int J Appl Earth Obs Geoinf* 80:145–156. <https://doi.org/10.1016/j.jag.2019.04.016>
- Lorenz K, Lal R, Ehlers K (2019) Soil organic carbon stock as an indicator for monitoring land and soil degradation in relation to United Nations' Sustainable Development Goals. *Land Degrad Dev* 30:824–838. <https://doi.org/10.1002/ldr.3270>
- Loupasakis C (2020) Contradictive mining–induced geocatastrophic events at open pit coal mines: the case of Amintaio coal mine, West Macedonia. *Greece Arab J Geosci* 13(13):1–2. <https://doi.org/10.1007/s12517-020-05633-y>
- Lynden GWJ, Oldeman LR (1997) The assessment of the status of human-induced soil degradation in South and Southeast Asia. ISRIC, International Soil Reference and Information Centre, Wageningen
- Maity B, Mallick SK, Rudra S (2020) Spatiotemporal dynamics of urban landscape in Asansol municipal corporation, West Bengal, India: a geospatial analysis. *GeoJournal*. <https://doi.org/10.1007/s10708-020-10315-z>
- Majkowska A, Kolendowicz L, Pórolniczak M, Hauke J, Czernecki B (2017) The urban heat island in the city of Poznań as derived from Landsat 5 TM. *Theor Appl Climatol* 128(3–4):769–783. <https://doi.org/10.1007/s00704-016-1737-6>
- Manjunatha MC, Basavarajappa HT (2020) Mapping of land units and its change detection analysis in Chitradurga taluk of Karnataka State, India using geospatial technology. *Int Adv Res J Sci Eng Technol* 7(7):61–68
- Masoudi M (2014) Risk assessment of vegetation degradation using GIS. *J Agric Sci Technol* 16:1711–1722

- Masoudi M, Amiri E (2015) A new model for hazard evaluation of vegetation degradation using DPSIR framework, a case study: Sadra region, Iran. *Pol J Ecol* 63:1–9. <https://doi.org/10.3161/15052249PJE2015.63.1.001>
- Masoudi M, Zakeri Nejad R (2010) Hazard assessment of desertification using MEDALUS model in Mazayjan plain, Fars province, Iran. *Ecol Environ Conserv* 16:425–430
- Matchanov M, Teodoro A, Schroder C (2016) Criterion definition for the identification of physical–geographical boundaries of Khorezm oasis through remotely sensed data. *Environ Monit Assess* 188(1):1–14. <https://doi.org/10.1007/s10661-015-5035-z>
- Matin S, Ghosh S, Behera MD (2018) Land transformation and associated degradation in Indian Ganga River Basin using forest cover land use mapping and residual trend analysis. *J Arid Land*. <https://doi.org/10.1007/s40333-018-0106-y>
- Milanović M, Tomić M, Perović V, Radovanović M, Mukherjee S, Jakšić D, Petrović M, Radovanović A (2017) Land degradation analysis of mine-impacted zone of Kolubara in Serbia. *Environ Earth Sci* 76(16):1–10. <https://doi.org/10.1007/s12665-017-6896-y>
- Moawad BM (2012) Geoscience general tool package. Max-Planck Institute für Chemie, Mainz
- Mohajane M, Essahlaoui A, Oudija F, El Hafyani M, Cláudia Teodoro A (2017) Mapping forest species in the central middle atlas of Morocco (Azrou Forest) through remote sensing techniques. *ISPRS Int J Geo Inf* 6(9):275. <https://doi.org/10.3390/ijgi6090275>
- Mohamed E, Belal AA, Ali RR, Saleh A, Hendawy EA (2019) Land degradation. In: El-Ramady H, Alshaal T, Bakr N, Elbana T, Mohamed E, Belal A (eds) *The soils of Egypt*. Springer, Cham, pp 159–174
- Mohapatra SN, Pani P, Sharma M (2014) Rapid urban expansion and its implications on geomorphology: a remote sensing and GIS based study. *Geogr J* 44:342–376
- Mohd Ayob N, Ismail N, Masron T (2015) Traditional and local ecological knowledge for land use mapping. *Appl Mech Mater* 747:306–309. <https://doi.org/10.4028/www.scientific.net/AMM.747.306>
- Mu Q, Heinsch FA, Zhao M, Running SW (2007) Development of a global evapotranspiration algorithm based on MODIS and global meteorology data. *Remote Sens Environ* 11:519–536
- Mueller T, Dressler G, Tucker C, Pinzon J, Leimgruber P, Dubayah R, Hurr G, Böhning-Gaese K, Fagan W (2014) Human land-use practices lead to global long-term increases in photosynthetic capacity. *Remote Sens* 6:5717–5731. <https://doi.org/10.3390/rs6065717>
- Neigh CSR, Tucker CJ, Townshend JRG (2008) North American vegetation dynamics observed with multi-resolution satellite data. *Remote Sens Environ* 112:1749–1772. <https://doi.org/10.1016/j.rse.2007.08.018>
- Oldeman L, Hakkeling R, Sombroek W (1991) World map of the status of human-induced soil degradation. An explanatory note. International Soil Reference and Information Centre
- Owen TW, Carlson TN, Gillies RR (1998) An assessment of satellite remotely sensed land cover parameters in quantitatively describing the climatic effect of urbanization. *Int J Remote Sens* 19:1663–1681. <https://doi.org/10.1080/014311698215171>
- Pacheco FAL, Fernandes LFS, Junior RFV, Valera CA, Pissarra TCT (2018) Land degradation: multiple environmental consequences and routes to neutrality. *Curr Opin Environ Sci Health* 5:79–86. <https://doi.org/10.1016/j.coesh.2018.07.002>
- Parida AK, Das AB, Mitra B (2004) Effects of salt on growth, ion accumulation, photosynthesis and leaf anatomy of the mangrove, *Bruguiera parviflora*. *Trees* 18:167–174. <https://doi.org/10.1007/s00468-003-0293-8>
- Rahaman S, Kumar P, Chen R, Meadows ME, Singh RB (2020) Remote sensing assessment of the impact of land use and land cover change on the environment of Bardhaman district, West Bengal, India. *Front Environ Sci*. <https://doi.org/10.3389/fenvs.2020.00127>
- Rouse JW, Haas RH, Schell JA, Deering DW (1974) Monitoring vegetation systems in the Great Plains with ERTS. In: *Third ERTS symposium*, NASA SP-351, Washington DC, pp 309–317
- Saha A, Patil M, Goyal VC, Rathore DS (2018) Assessment and impact of soil moisture index in agricultural drought estimation using remote sensing and GIS techniques. In: *Multidisciplinary digital publishing institute proceedings*, vol 7, no 1, p 2. <https://doi.org/10.3390/ECWS-3-05802>
- Sepehr A, Hassanli A, Ekhtesasi M, Jamali J (2007) Quantitative assessment of desertification in south of Iran using MEDALUS method. *Environ Monit Assess* 134(1):243–254. <https://doi.org/10.1007/s10661-007-9613-6>
- Seto KC, Fragkias M, Güneralp B, Reilly MK (2011) A meta-analysis of global urban land expansion. *PLoS One* 6(8):e23777. <https://doi.org/10.1371/journal.pone.0023777>
- Shalaby A, Tateishi R (2007) Remote sensing and GIS for mapping and monitoring land cover and land-use changes in the Northwestern coastal zone of Egypt. *Appl Geogr* 27(1):28–41. <https://doi.org/10.1016/j.apgeog.2006.09.004>
- Shih SF, Jordan JD (1993) Use of Landsat thermal-IR data and GIS in soil moisture assessment. *J Irrig Drain Eng* 119(5):868–879. [https://doi.org/10.1061/\(ASCE\)0733-9437\(1993\)119:5\(868\)](https://doi.org/10.1061/(ASCE)0733-9437(1993)119:5(868))
- Siddique G, Roy A, Mandal MH, Ghosh S, Basak A, Singh M, Mukherjee N (2020) An assessment on the changing status of urban green space in Asansol city, West Bengal. *GeoJournal*. <https://doi.org/10.1007/s10708-020-10312-2>
- Silleos NG, Alexandridis TK, Gitas IZ, Perakis K (2006) Vegetation indices: advances made in biomass estimation and vegetation monitoring in the last 30 years. *Geocarto Int* 21(4):21–28. <https://doi.org/10.1080/10106040608542399>
- Sklenicka P (2016) Classification of farmland ownership fragmentation as a cause of land degradation: a review on typology, consequences, and remedies. *Land Use Policy* 57:694–701. <https://doi.org/10.1016/j.landusepol.2016.06.032>
- Song Y, Ma M (2011) A statistical analysis of the relationship between climatic factors and the normalized difference vegetation index in China. *Int J Remote Sens* 32(14):3947–3965. <https://doi.org/10.1080/01431161003801336>
- Souto J, Beltrão N, Teodoro A (2019) Performance of remotely sensed soil moisture for temporal and spatial analysis of rainfall over Sao Francisco River basin, Brazil. *Geosciences* 9(3):144. <https://doi.org/10.3390/geosciences9030144>
- Story M, Congalton RG (1986) Accuracy assessment: a user's perspective. *Photogramm Eng Remote Sens* 52(3):397–399
- Taddese G (2001) Land degradation: a challenge to Ethiopia. *Environ Manag* 27(6):815–824. <https://doi.org/10.1007/s002670010190>
- Teodoro A, Santos P, Espinha Marques J, Ribeiro J, Mansilha C, Melo A, Flores D (2021) An integrated multi-approach to environmental monitoring of a self-burning coal waste pile: the São Pedro da Cova Mine (Porto, Portugal) study case. *Environments* 8(6):48. <https://doi.org/10.3390/environments8060048>
- Thiam AK (2003) The causes and spatial pattern of land degradation risk in southern Mauritania using multitemporal AVHRR-NDVI imagery and field data. *J Land Degrad Dev* 14:133–142. <https://doi.org/10.1002/ldr.533>
- UNCCD (1994) United Nations Convention to Combat Desertification. Elaboration an int convention combat desertification countries experiencing serious drought and/or desertification, particularly Afr (U.N. Doc. A/AC.241/27, 33 I.L.M. 1328, United Nations)
- Urqueta H, Jódar J, Herrera C, Wilke HG, Medina A, Urrutia J, Rodríguez J (2018) Land surface temperature as an indicator of the unsaturated zone thickness: a remote sensing approach in the

- Atacama Desert. *Sci Total Environ* 612:1234–1248. <https://doi.org/10.1016/j.scitotenv.2017.08.305>
- Vlek PLG, Le QB, Tamene L (2008) Land decline in land-rich Africa: a creeping disaster in the making. CGIAR Science Council Secretariat, Rome
- Vlek PL, Le QB, Tamene L (2010) Assessment of land degradation, its possible causes and threat to food security in Sub-Saharan Africa. Food security and soil quality. CRC Press, Boca Raton, pp 57–86
- Voogt JA, Oke TR (2003) Thermal remote sensing of urban climate. *Remote Sens Environ* 86:370–384. [https://doi.org/10.1016/S0034-4257\(03\)00079-8](https://doi.org/10.1016/S0034-4257(03)00079-8)
- Walawender JP, Szymanowski M, Hajto MJ, Bokwa A (2014) Land surface temperature patterns in the urban agglomeration of Krakow (Poland) derived from Landsat-7/ETM+ data. *Pure Appl Geophys* 171:913–940. <https://doi.org/10.1007/s00024-013-0685-7>
- Yue W, Xu J, Tan W, Xu L (2007) The relationship between land surface temperature and NDVI with remote sensing: application to Shanghai Landsat 7 ETM+ data. *Int J Remote Sens* 28(15):3205–3226. <https://doi.org/10.1080/01431160500306906>
- Zhang C, Lu D, Chen X, Zhang Y, Maisupova B, Tao Y (2016) The spatiotemporal patterns of vegetation coverage and biomass of the temperate deserts in Central Asia and their relationships with climate controls. *Remote Sens Environ* 175:271–281. <https://doi.org/10.1016/j.rse.2016.01.002>
- Zhang Y, Odeh IOA, Han C (2009) Bi-temporal characterization of land surface temperature in relation to impervious surface area, NDVI and NDBI, using a sub-pixel image analysis. *Int J Appl Earth Obs* 11(4):256–264. <https://doi.org/10.1016/j.jag.2009.03.001>

Publisher's Note Springer Nature remains neutral with regard to jurisdictional claims in published maps and institutional affiliations.